ResearchGate

See discussions, stats, and author profiles for this publication at: https://www.researchgate.net/publication/242316976

Modeling Transient Heat Transfer Using SPH and Implicit Time Integration

Article *in* Numerical Heat Transfer Fundamentals · January 2007

DOI: 10.1080/10407790600762763

CITATIONS
74

READS
2,811

3 authors, including:

Mehmet Yildiz
Sabanci University
235 PUBLICATIONS **3,669** CITATIONS
SEE PROFILE

S. Dost
University of Victoria
294 PUBLICATIONS **3,360** CITATIONS
SEE PROFILE

Some of the authors of this publication are also working on these related projects:

EHD based multiphase flow View project

Numerical simulation of jet electrified printing View project

All content following this page was uploaded by Mehmet Yildiz on 08 April 2014.

The user has requested enhancement of the downloaded file.

This article was downloaded by:[ANKOS Consortium]
On: 18 January 2008
Access Details: [subscription number 772815469]
Publisher: Taylor & Francis
Informa Ltd Registered in England and Wales Registered Number: 1072954
Registered office: Mortimer House, 37-41 Mortimer Street, London W1T 3JH, UK

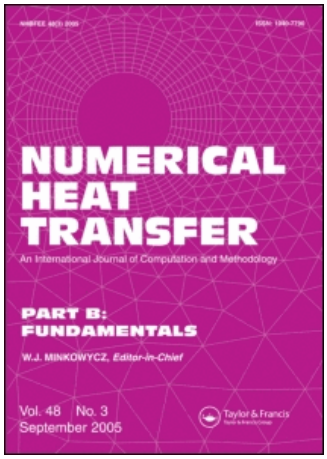

Numerical Heat Transfer, Part B: Fundamentals
An International Journal of Computation and Methodology
Publication details, including instructions for authors and subscription information:
http://www.informaworld.com/smpp/title~content=t713723316

Modeling Transient Heat Transfer Using SPH and Implicit Time Integration

Rusty Rook [a]; Mehmet Yildiz [a]; Sadik Dost [a]
[a] Crystal Growth Lab, Department of Mechanical Engineering, University of Victoria, Victoria, British Columbia, Canada

Online Publication Date: 01 January 2007
To cite this Article: Rook, Rusty, Yildiz, Mehmet and Dost, Sadik (2007) 'Modeling Transient Heat Transfer Using SPH and Implicit Time Integration', Numerical Heat Transfer, Part B: Fundamentals, 51:1, 1 - 23
To link to this article: DOI: 10.1080/10407790600762763
URL: http://dx.doi.org/10.1080/10407790600762763

PLEASE SCROLL DOWN FOR ARTICLE

Full terms and conditions of use: http://www.informaworld.com/terms-and-conditions-of-access.pdf

This article maybe used for research, teaching and private study purposes. Any substantial or systematic reproduction, re-distribution, re-selling, loan or sub-licensing, systematic supply or distribution in any form to anyone is expressly forbidden.

The publisher does not give any warranty express or implied or make any representation that the contents will be complete or accurate or up to date. The accuracy of any instructions, formulae and drug doses should be independently verified with primary sources. The publisher shall not be liable for any loss, actions, claims, proceedings, demand or costs or damages whatsoever or howsoever caused arising directly or indirectly in connection with or arising out of the use of this material.

Numerical Heat Transfer, Part B, 51: 1–23, 2007
Copyright © Taylor & Francis Group, LLC
ISSN: 1040-7790 print/1521-0626 online
DOI: 10.1080/10407790600762763

Downloaded By: [ANKOS Consortium] At: 10:15 18 January 2008

MODELING TRANSIENT HEAT TRANSFER USING SPH AND IMPLICIT TIME INTEGRATION

Rusty Rook, Mehmet Yildiz, and Sadik Dost
Crystal Growth Lab, Department of Mechanical Engineering, University of Victoria, Victoria, British Columbia, Canada

In this article, a two-dimensional transient heat conduction problem is modeled using smoothed particle hydrodynamics (SPH) with a Crank-Nicolson implicit time integration technique. The main feature of this work is that it applies implicit time stepping, an unconditionally stable Crank-Nicolson approach, in the thermal conduction simulation of liquid-phase diffusion (LPD) semiconductor crystal growth. This SPH simulation is compared with the equivalent finite-volume results. As well, two transient thermal conduction test problems are simulated using both explicit and Crank-Nicolson schemes, and their results compared with the analytical solutions. One of the current drawbacks of SPH is that explicit time-stepping algorithms, such as predictor-corrector methods or leapfrog methods, require extremely small time steps for a stable simulation. Using implicit time integration opens SPH up to a much larger class of practical problems in applied mechanics.

1. INTRODUCTION

Smoothed particle hydrodynamics (SPH) is an adaptive, mesh-free, Lagrangian numerical approximation technique used for modeling physical problems. Unlike Eulerian computational techniques such as the finite-volume and finite-difference methods, SPH does not require a grid, as derivatives are approximated using a kernel function. Each ''particle'' in the domain can be associated with one discrete physical object, or it may represent a macroscopic part of the continuum [1]. The continuum is represented by an ensemble of particles each carrying mass, momentum, and other hydrodynamic properties. In recent years, several other mesh-free methods have been gaining popularity in the literature, such as the meshless element-free Galerkin (EFG) method [2–5], moving least-square methods [6], or the diffuse approximation method [7]. However, these approaches tend to be formulated in a Eulerian frame. The Lagrangian framework of SPH is convenient for simulations involving interfacial surfaces, such as in the field of semiconductor crystal growth. For this application, the finite-volume approach is difficult to implement, as the computational mesh is required to adapt to the crystal growth surface. Although originally proposed to handle cosmological simulations [8, 9], SPH has become increasingly generalized to

Received 8 November 2005; accepted 31 March 2006.
Funding provided by the Natural Sciences and Engineering Research Council and the Canada Research Chairs is greatfully acknowledged.
Address correspondence to Sadik Dost, Crystal Growth Lab, Department of Mechanical Engineering, University of Victoria, Victoria, BC V8W 3P6, Canada. E-mail: sdost@me.uvic.ca

Downloaded By: [ANKOS Consortium] At: 10:15 18 January 2008

NOMENCLATURE

a_n	kernel dimension coefficients
A_{ij}	interaction coefficient
c_i	speed of sound for particle i
c_p	specific heat capacity
C_{CFL}	Courant coefficient
$f(x_i^\beta)$	arbitrary position function
$\langle f(x_i^\beta)\rangle$	SPH approximation of $f(x_i^\beta)$
g	determinant of $g_{\alpha\beta}$
$g_{\alpha\beta}$	metric tensor
h, h_{ij}	smoothing length
H	domain height
$\mathcal{H}$	convective heat transfer coef.
$\overline{\mathcal{H}}$	modified heat transfer coef.
L	domain length
m_i	mass of particle i
N	total number of particles
R	radius
t	time
Δt	time increment
T	temperature
T_f	ambient furnace temperature
$W(x_{ij}, h)$	kernel function
x_i^α	position vector of i
x_{ij}^α	positional difference
x_{ij}	magnitude of x_{ij}^α
(x, y, z)	Cartesian coord.
α_D	diffusivity
β_k	series coefficient
γ_l	series coefficient
$\delta^3(x_{ij}^\beta)$	3-D Kronecker delta
κ	conductivity
κ_S	solid conductivity
ρ	density

Subscripts

i, j	particle indices
0	reference state

Superscripts

m	time-step index
$\alpha, \beta, \gamma, \lambda$	component indices

handle many types of fluid and solid mechanics problems [10–13]. SPH advantages include relatively easy modeling of complex material surface behavior, as well as simple implementation of more complicated physics, such as solidification [14].

In many applications, such as crystal growth [15–17], systems must be simulated as they evolve over a period of several minutes or hours. A review of SPH literature reveals that SPH has not yet been applied to solve practical problems involving large time scales. The explicit-time-step algorithms currently used in SPH simulations require miniscule time steps for a stable solution, putting the SPH method out of reach for many computational fluid dynamics (CFD) problems. If implicit time stepping was incorporated in SPH, the range of applicability would greatly increase. Other sources in the literature have encorporated implicit and semi-implicit time integration [18], but to our knowledge it has not yet been investigated in crystal growth applications.

The SPH technique computes discrete particle properties using a smoothing, *kernel* distribution function to account for the effects of surrounding particles. It is assumed that the properties characteristic of the particle of interest are influenced by all other particles in the global domain. However, one approximation of SPH is to include only the effects of nearby particles, within a smoothing radius denoted $2h$. The length h defines the *support domain* of the particle of interest (i.e., a localized domain over which the kernel will be nonzero). Throughout the present simulations, the compactly supported cubic spline kernel

$$W(x_{ij}, h) = a_n \begin{cases} \frac{2}{3} - \left(\frac{x_{ij}}{h}\right)^2 + \frac{1}{2}\left(\frac{x_{ij}}{h}\right)^3 & \text{if } 0 \le x_{ij} < h \\ \frac{1}{6}\left(2 - \left(\frac{x_{ij}}{h}\right)^3\right) & \text{if } h \le x_{ij} < 2h \\ 0 & \text{if } x_{ij} \ge 2h \end{cases} \tag{1}$$

Downloaded By: [ANKOS Consortium] At: 10:15 18 January 2008

was employed, where x_{ij} is the magnitude of the distance between particles i and j. In Eq. (1), n is the dimension of the space, and the coefficient a_n is dependent on the smoothing length h and has values

$$a_1 = \frac{1}{h} \quad a_2 = \frac{15}{7\pi h^2} \quad a_3 = \frac{3}{2\pi h^3}$$

in one, two, and three dimensions, respectively. For $h = 1$, the cubic spline kernel disribution of Eq. (1) is illustrated for a two-dimensional (x_{ij}^1, x_{ij}^2) Cartesian domain in Figure 1.

For clarity, it is worthwhile taking a moment to state explicitly the notational conventions that will be used throughout this article. All vector quantities will be written using the index notation, with Greek indices denoting the tensor components exclusively. These components will always be written in contravariant form as superscripts. As well, throughout this article, the Einstein summation convention is employed, where any repeated index is summed over the range of the index. Latin indices (i, j) will be used to denote particles, and will always be placed as subscripts. For example, the n-dimensional vector denoting the position of particle i is written as

$$\vec{\mathbf{x}}_i \rightarrow x_i^\alpha \text{ for } \alpha = 1, 2, \ldots, n \tag{2}$$

As well, we will employ the concise $(\ )_{ij}$ difference notation,

$$x_{ij}^\alpha \equiv x_i^\alpha - x_j^\alpha \text{ where } x_{ij} \equiv \left\| x_i^\alpha - x_j^\alpha \right\| = \sqrt{g_{\alpha\beta} x_{ij}^\alpha x_{ij}^\beta}$$

is the magnitude of the distance between particles i and j written in a curvilinear coordinate system in terms of the metric tensor $g_{\alpha\beta}$.

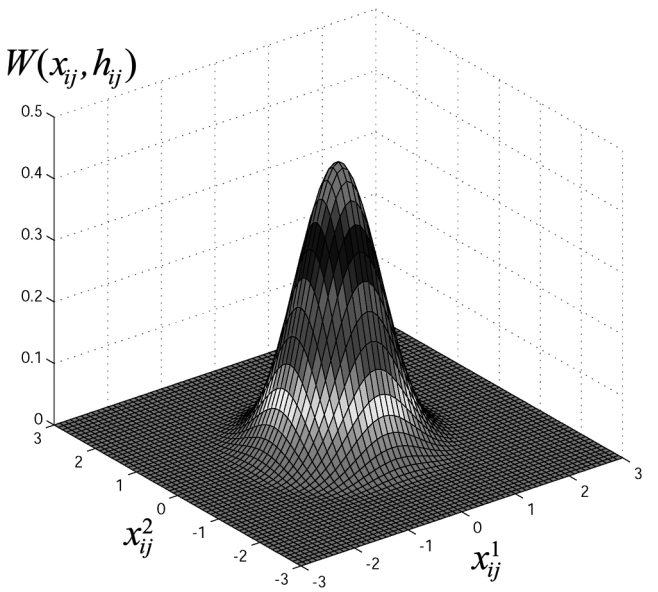

Figure 1. A 2-D cubic spline kernel.

Downloaded By: [ANKOS Consortium] At: 10:15 18 January 2008

For two-dimensional thermal conduction in Cartesian coordinates, the governing equation for the evolution of the temperature field $T = T(x, y, t)$ is

$$\rho c_p \frac{\partial T}{\partial t} = \kappa g^{\alpha\beta} T_{;\alpha\beta} \Rightarrow \frac{\partial T}{\partial t} = \alpha_D \cdot \left(\frac{\partial^2 T}{\partial x^2} + \frac{\partial^2 T}{\partial y^2} \right) \tag{3}$$

where c_p is the specific heat, κ is the (constant) thermal conductivity, ρ is the material density, and $\alpha_D = \kappa / \rho c_p$ is the thermal diffusivity. The quantity $g^{\alpha\beta} T_{;\alpha\beta}$ is the Laplacian of the temperature field in general curvilinear coordinates in terms of the second covariant derivative operator $(\,)_{;\alpha\beta}$ and the conjugate metric tensor $g^{\alpha\beta}$.

2. SMOOTHED PARTICLE HYDRODYNAMICS

The three-dimensional Dirac delta function $\delta^3(x_{ij}^{\beta})$ is the starting point for the SPH approximation technique. This function satisfies the identity

$$f(x_i^{\beta}) = \int\int\int_{\Omega} f(x_j^{\beta}) \delta^3(x_{ij}^{\beta}) d\Omega \tag{4}$$

where $d\Omega = \sqrt{g} dx^1 dx^2 dx^3 = \sqrt{g} dx^{\beta}$ is a differential volume element. The fundamental approximation of SPH is to replace the Dirac delta function with the even kernel function $W(x_{ij}, h)$. We then write the fundamental SPH approximation in three dimensions as

$$f(x_i^{\beta}) \approx \langle f(x_i^{\beta}) \rangle \equiv \int\int\int_{\Omega} f(x_j^{\beta}) W(x_{ij}, h) d\Omega \tag{5}$$

where $\langle f(x_i^{\beta}) \rangle$ is the kernel approximation of the scalar field $f(x_i^{\beta})$ at particle i.

2.1. Spatial Derivatives in SPH

Since SPH is an approximation technique, there are several different ways of approximating spatial derivatives. In this section, we present SPH approximations for the gradient of a scalar function, and the Laplacian of a scalar function.

In order to determine the SPH approximation for the gradient of a scalar function, we make the substitution $f(x_j^{\beta}) \rightarrow f_{;\alpha_j}(x_j^{\beta})$ in Eq. (5) to produce

$$\langle f_{;\alpha}(x_i^{\beta}) \rangle = \int\int\int_{\Omega} f_{;\alpha_j}(x_j^{\beta}) W(x_{ij}, h) d\Omega$$

where the covariant differentiations takes place referencing x_i^{β} coordinates using the $(\,)_{;\alpha}$ operator, and x_j^{β} coordinates using the $(\,)_{;\alpha_j}$ operator. Upon integrating by

Downloaded By: [ANKOS Consortium] At: 10:15 18 January 2008

parts, and noting that $W_{;\alpha}(x_{ij},h) = -W_{;\alpha_j}(x_{ij},h)$, it can be shown that

$$\langle f_{;\alpha}(x_i^\beta)\rangle = \int\int\int_\Omega f(x_j^\beta) W_{;\alpha}(x_{ij},h) d\Omega \tag{6}$$

for all interior particles i. In the present article, the error introduced by the kernel truncation of near-boundary interior particles has been neglected. This result is especially significant, since it states that the spatial derivatives of particle properties can be found simply by differentiation of the kernel.

The SPH Laplacian of a scalar field $f_{;\gamma\lambda}(x_i^\beta)$ is derived in the Appendix, and is given as

$$\langle g^{\gamma\lambda} f_{;\gamma\lambda}(x_i^\beta)\rangle = 2\int\int\int_\Omega \frac{\left[f(x_i^\beta) - f(x_j^\beta)\right] x_{ij}^\alpha}{g_{\mu\nu} x_{ij}^\mu x_{ij}^\nu} W_{;\alpha}(x_{ij},h) d\Omega \tag{7}$$

in terms of the gradient of the kernel, where all covariant derivatives in the above equation are with respect to x_i^β coordinates.

2.2. Particle Approximations in SPH

Recall that Eq. (5) is the SPH approximation for a continuous distribution. If, however, we recognize that this integration will be carried out over all N discrete particles within the domain, we can discretize Eq. (5) as

$$\langle f(x_i^\beta)\rangle = \sum_{j=1}^{N} \frac{m_j}{\rho_j} f(x_j^\beta) W(x_{ij},h) \tag{8}$$

to produce the SPH approximation of a field property $f(x^\beta)$ at particle i in terms of all other interacting particles j, and a representative particle volume written in terms of particle mass m_j and particle density ρ_j.

In the following simulations, the discrete SPH particle appoximation used for the gradient of a scalar function is

$$\langle f_{;\alpha}(x_i^\beta)\rangle = \sum_{j=1}^{N} \frac{m_j}{\rho_i} \left[f(x_j^\beta) - f(x_i^\beta)\right] W_{;\alpha}(x_{ij},h) \tag{9}$$

The discrete form of the SPH approximation for the Laplacian of a scalar function is written from discretization of Eq. (7) as

$$\langle g^{\gamma\lambda} f_{;\gamma\lambda}(x_i^\beta)\rangle = 2\sum_{j=1}^{N} \frac{m_j}{\rho_j} \frac{[f(x_i^\beta) - f(x_j^\beta)]}{x_{ij}} \frac{\partial W(x_{ij},h)}{\partial x_{ij}} \tag{10}$$

Downloaded By: [ANKOS Consortium] At: 10:15 18 January 2008

3. EXPLICIT AND IMPLICIT TIME-STEPPING USING THE CRANK-NICOLSON ALGORITHM

In order to increment the time step Δt in a numerical simulation, one can use either an explicit or an implicit scheme.

3.1. Explicit Time Stepping

Explicit schemes are the most straightforward to apply, but are notoriously susceptible to instabilities when Δt becomes too great. For example, the time discretization of Eq. (3) using the most straightforward explicit approach is

$$\frac{T_i^{m+1} - T_i^m}{\Delta t} = 2\alpha_{Di} \sum_{\substack{j=1 \\ j \neq i}}^{N} \frac{m_j}{\rho_j} \frac{(T_i^m - T_j^m)}{x_{ij}} \frac{\partial W(x_{ij}, h)}{\partial x_{ij}}$$

where we have used Eq. (10) for the SPH approximation for the Laplacian of the temperature field, and the superscript m denotes the time step. Rearranging the above equation, we have that

$$T_i^{m+1} = T_i^m + 2\alpha_{Di}\,\Delta t \sum_{\substack{j=1 \\ j \neq i}}^{N} \frac{m_j}{\rho_j} \frac{(T_i^m - T_j^m)}{x_{ij}} \frac{\partial W(x_{ij}, h)}{\partial x_{ij}} \tag{11}$$

which is an SPH equation used to solve for the temperature distribution at the discrete time step $m + 1$. In three-dimensional simulations, the quantity m_j/ρ_j represents the particle volume. However, for the two-dimensional problems considered, this quantity is interpreted as a characteristic particle area. Since the particles are equally spaced, the particle area is approximated by dividing the domain area by the number of particles. Monaghan and Cleary have reported [19] that for pure conduction problems, the time step for an explicit scheme must satisfy

$$\Delta t \leq 0.15 \frac{h^2}{\alpha_D} \tag{12}$$

for a stable solution. Since in the following simulations we have taken $h = 0.25$ cm and $\alpha_D = 1\,\text{cm}^2/\text{s}$, the time step is restricted to $\Delta t \leq 0.009$ s to ensure an accurate solution.

In more complicated models where particles move, the explicit leapfrog algorithm [20] can be used to break down the thermomechanical balance laws (conservation of mass, momentum, and energy) into discrete time steps. The algorithm stability is controlled by the Courant-Friedrichs-Lewy (CFL) condition, where the recommended time step is

$$\Delta t \leq C_{CFL} \frac{h}{\max(c_i + \|v_i^\alpha\|)} \tag{13}$$

Downloaded By: [ANKOS Consortium] At: 10:15 18 January 2008

where C_{CFL} is a constant between 0 and 1, v_i^{α} is the particle velocity, and c_i is the speed of sound for the particle material. The CFL condition is a major drawback of using an explicit-time-step approach, as Δt is usually required to be extremely small. This fact makes the leapfrog technique well suited to problems involving only very small time scales. However, for simulations involving large time scales, explicit approaches such as the leapfrog technique are not suitable.

3.2. Implicit Crank-Nicolson Time Stepping

It is well known that implicit time-stepping approaches, such as the Crank-Nicolson approach, are unconditionally stable with respect to choice of Δt. Using a simple implicit approach, Eq. (11) has the right-hand side modified to read

$$T_i^{m+1} = T_i^m + 2\alpha_{Di}\,\Delta t \sum_{\substack{j=1 \\ j\neq i}}^{N} \frac{m_j}{\rho_j} \frac{(T_i^{m+1} - T_j^{m+1})}{x_{ij}} \frac{\partial W(x_{ij}, h_{ij})}{\partial x_{ij}} \tag{14}$$

where now there is no longer an explicit equation for the temperature of particle i at time step $m+1$. Instead of solving systematically for each temperature T_i^{m+1} as was done in the explicit scheme, with the implicit approach we must now solve the *system of equations*

$$T_i^{m+1}\left[1 - \sum_{\substack{j=1 \\ j\neq i}}^{N} A_{ij}\right] + \sum_{\substack{j=1 \\ j\neq i}}^{N} A_{ij} T_j^{m+1} = T_i^m \tag{15}$$

where

$$A_{ij} \equiv 2\alpha_{Di}\,\Delta t \frac{m_j}{\rho_j} \frac{1}{x_{ij}} \frac{\partial W(x_{ij}, h_{ij})}{\partial x_{ij}} \tag{16}$$

is a dimensionless parameter characterizing the relationship between particles i and j. Here, at each time step $m+1$, a matrix must be inverted.

Alternatively, the Crank-Nicolson implicit technique is described by

$$\begin{aligned} T_i^{m+1} = T_i^m &+ \alpha_{Di}\,\Delta t \sum_{\substack{j=1 \\ j\neq i}}^{N} \frac{m_j}{\rho_j} \frac{(T_i^{m+1} - T_j^{m+1})}{x_{ij}} \frac{\partial W(x_{ij}, h_{ij})}{\partial x_{ij}} \\ &+ \alpha_{Di}\,\Delta t \sum_{\substack{j=1 \\ j\neq i}}^{N} \frac{m_j}{\rho_j} \frac{(T_i^m - T_j^m)}{x_{ij}} \frac{\partial W(x_{ij}, h_{ij})}{\partial x_{ij}} \end{aligned} \tag{17}$$

This system of equations is rewritten and solved in the form

$$T_i^{m+1}\left[1 - \sum_{\substack{j=1 \\ j\neq i}}^{N} \frac{A_{ij}}{2}\right] + \sum_{\substack{j=1 \\ j\neq i}}^{N} \frac{A_{ij}}{2} T_j^{m+1} = T_i^m \left[1 + \sum_{\substack{j=1 \\ j\neq i}}^{N} \frac{A_{ij}}{2}\right] - \sum_{\substack{j=1 \\ j\neq i}}^{N} \frac{A_{ij}}{2} T_j^m \tag{18}$$

Downloaded By: [ANKOS Consortium] At: 10:15 18 January 2008

where A_{ij} is defined from Eq. (16). Equation (18) gives the Crank-Nicolson solution to the temperature of a given particle i at time $m+1$. The unknown temperatures T_i^{m+1} and T_j^{m+1} (consisting of all j neighboring particles of i) have been grouped to the left-hand side of Eq. (18). All quantities on the right-hand side are known, since the particle temperatures at time step m are determined. Therefore, for a total number of particles N, Eq. (18) produces $i = 1, 2, \ldots, N$ equations for N unknowns. Since N is typically much greater than the number of particle neighbors for a given particle of interest i, this system of equations will contain mostly zeros, forming a sparse system. Several algorithms exist for the solution of the above system of equations, such as direct matrix inversion, Gauss-Siedel iteration, or the biconjugate gradient method. In terms of solution approaches, the biconjugate gradient method was found to outperform Gauss-Siedel iteration and direct matrix inversion in terms of convergence and efficiency. Further details on this approach can be found in the literature [21] and are discussed in the following section.

Note that for general CFD problems, the SPH particles will move, and both the distance between particles x_{ij} and the kernel derivatives $\partial W/\partial x_{ij}$ will require computation at time steps m and $m+1$, respectively. Indeed, the particle interactions make implementation of implicit time stepping more complicated in terms of solutions of the general Navier–Stokes equations.

For simulations involving static particles, however, like those in the present work, no distinction between time steps is required since particle positions do not evolve. Liquid-phase diffusion (LPD) semiconductor crystal growth is one such application, where a low Prandtl number for the system allows computation of the thermal field independent from the flow field.

Monaghan suggested [18] a pairwise implicit time-marching scheme for the treatment of a multiphase continuum such as a mixture of dust and gas. In this work, he resolved the coupling between the separate equations of motion for the dust and the gas by considering each interacting pair separately, rather than including contributions from all neighbor particles for the particle of interest. His pairwise approach is contrasted with the direct implicit method applied in the present work. For multiphase continua, the pairwise approach is advantageous over a direct implicit scheme, which will require solution of matrices with bands with a size about the number of the neighbor particles. However, if the pairwise interaction is utilized for the solution of the balance of momentum for a single-phase continuum, it is equivalent to direct implicit time integration, as investigated here.

4. TRANSIENT CONDUCTION MODELING

Two thermal conduction problems were solved and compared with known analytical solutions, set in a two-dimensional Cartesian domain $0 \le x \le L$ and $0 \le y \le H$, where $L = H = 10$ cm was selected. This (x, y) problem domain was modeled with SPH using $N = 1{,}600$ (a grid of 40×40) particles shown in Figure 2. Boundary particles are designated with the $*$ symbol, whereas interior particles use the $\circ$ symbol.

Downloaded By: [ANKOS Consortium] At: 10:15 18 January 2008

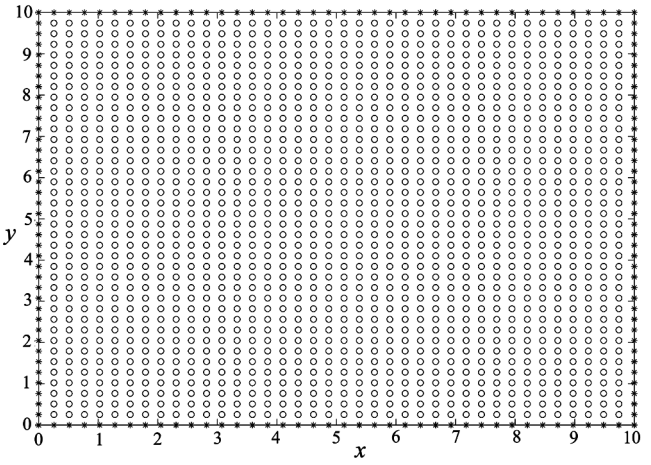

Figure 2. SPH test problem domain for $N = 1{,}600$ particles.

4.1. 2-D Transient Heat Conduction Problem 1

The first problem was to model the temperature profile $T(x, y, t)$ of the cooling of a plate at select times t. The plate was subjected to the boundary conditions

$$T(x, 0, t) = T(x, H, t) = T(0, y, t) = T(L, y, t) = T_1$$

and the initial condition

$$T(x, y, 0) = T_0$$

where T_0 is a uniform initial temperature throughout the domain. This domain is illustrated in the schematic in Figure 3.

For this simulation we use Eq. (3) and take the parameter values $\alpha_D = 1\text{cm}^2/\text{s}$, $T_0 = 100$, and $T_1 = 0^\circ\text{C}$. By separating variables, and applying the given boundary and initial conditions, an analytical solution to the temperature field $T(x, y, t)$ can be determined and given in terms of the double infinite series

$$T(x, y, t) = \frac{16T_0}{\pi^2} \sum_{k=1,3,\ldots}^{\infty} \sum_{l=1,3,\ldots}^{\infty} \frac{\exp\left[-\alpha_D \pi^2 \left(k^2/L^2 + l^2/H^2\right)t\right]}{kl} \sin\left(\frac{k\pi x}{L}\right) \sin\left(\frac{l\pi y}{H}\right) \tag{19}$$

Figure 4 illustrates the isothermal plots at times $t = 0.25$, $t = 1$, $t = 4$, and $t = 8\,\text{s}$ obtained from the analytical solution of Eq. (19) and the explicit time integration equation (11), where $T_0 = 100$ and $T_1 = 0^\circ\text{C}$. The SPH solution is represented by the dotted lines, and the analytical series solution by the solid lines. For the chosen domain of $N = 1{,}600$ particles, the representative particle area is found as $m_j/\rho_j \simeq 0.0625\ \text{cm}^2$, for $L = H = 10$ cm. The SPH solution correlates very well with

Downloaded By: [ANKOS Consortium] At: 10:15 18 January 2008

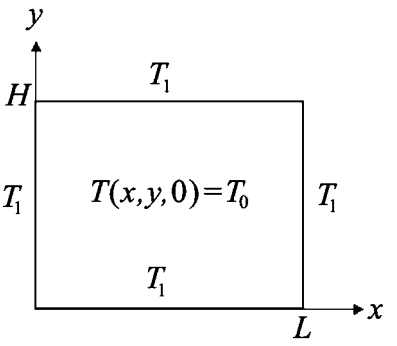

Figure 3. A 2-D (x, y) spatial domain with temperature boundary and initial conditions.

the known analytical solution for a smoothing length of $h = 0.25$ cm, $N = 1{,}600$ particles, and $\Delta t = 0.009$ s.

As expected, the explicit solution illustrated in Figure 4 was observed to break down as Δt was increased, in accordance with Eq. (12). However, the unconditional stability of the implicit time integration schemes permitted larger time steps, while the solution accuracy was maintained. It was found that the time step could be

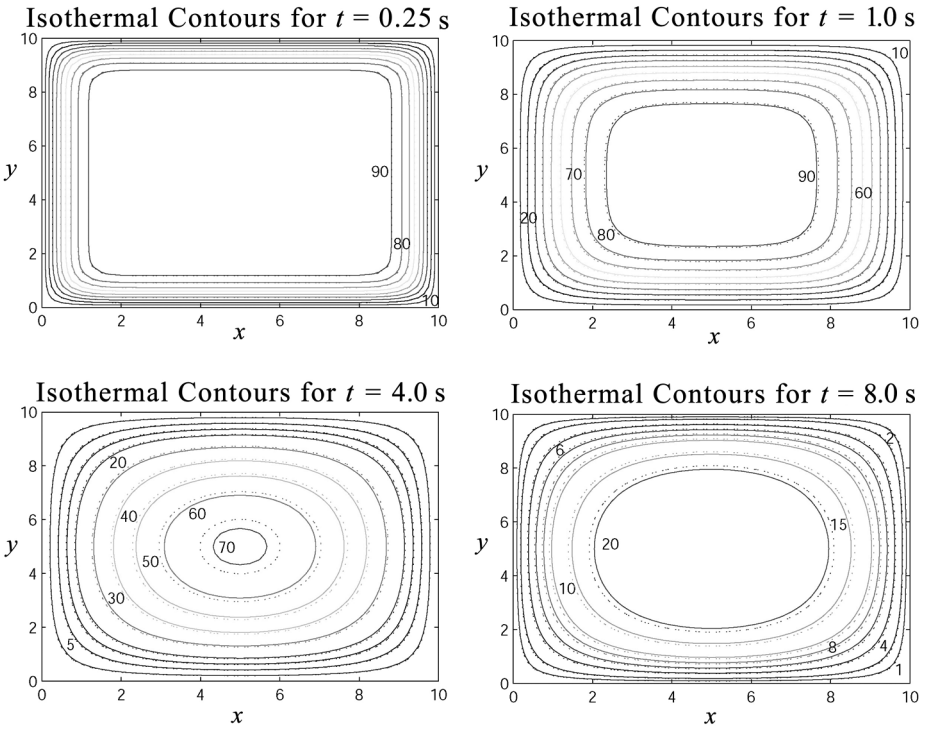

Figure 4. Analytical and explicit SPH isothermal contours at times $t = 0.25$, $t = 1$, $t = 4$, and $t = 8$ s found from Eqs. (19) and (11).

Downloaded By: [ANKOS Consortium] At: 10:15 18 January 2008

approximately doubled for the implicit schemes. A further increase in time step caused a significant reduction in solution accuracy.

Simulations to $t = 8\,\mathrm{s}$ using the implicit equation (15) and $\Delta t = 0.25\,\mathrm{s}$ took approximately 87 s of CPU time on a 64-bit AMD 3500+ processor, and the results are shown in Figure 5. These results correlate well with the explicit solution obtained in Figure 4.

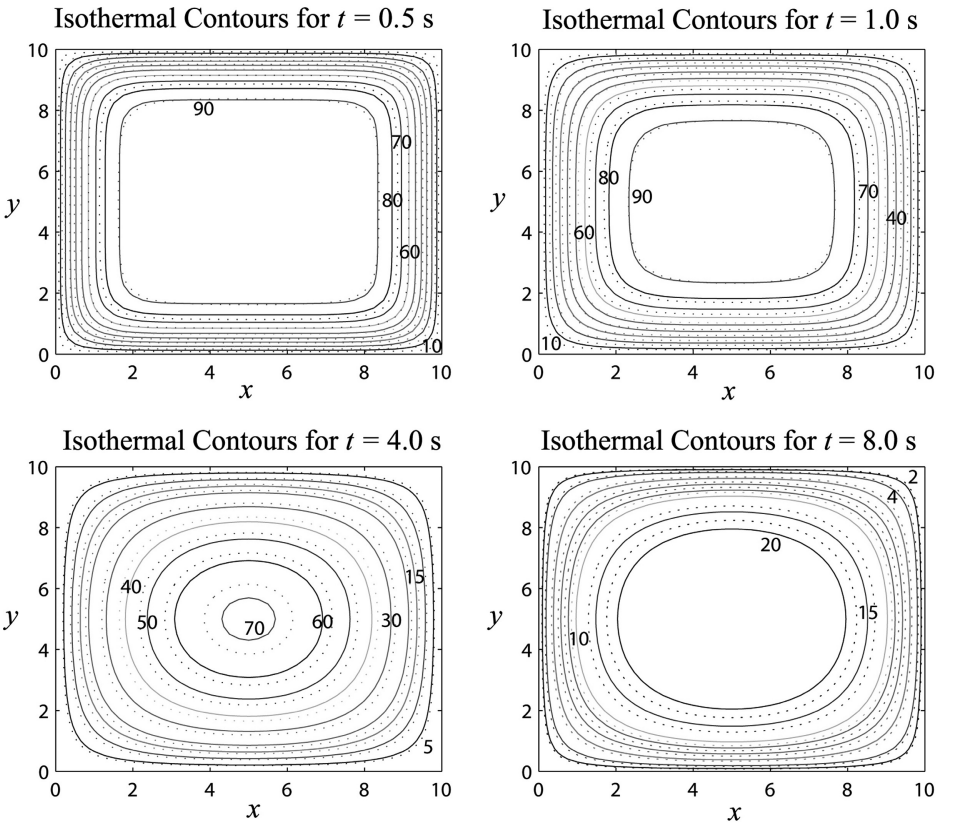

Figure 5. Analytical and implicit SPH isothermal contours at times $t = 0.25$, $t = 1$, $t = 4$, and $t = 8\,\mathrm{s}$ found from Eqs. (19) and (15).

4.2. 2-D Transient Heat Conduction Problem 2

The second simulation involved transient heat conduction with more complicated boundary conditions. Once again, the rectangular domain $0 \leq x \leq L$ and $0 \leq y \leq H$ was heated to an initial uniform temperature of $T(x, y, 0) = T_0$ with two insulated boundaries

$$\frac{\partial T(0, y, t)}{\partial x} = 0 \quad \frac{\partial T(x, 0, t)}{\partial y} = 0$$

Downloaded By: [ANKOS Consortium] At: 10:15 18 January 2008

and two boundaries that dissipate heat by convection to a medium at zero temperature,

$$\frac{\partial T(L,y,t)}{\partial x} = -\frac{\mathcal{H}}{\kappa} T(L,y,t) \quad \frac{\partial T(x,H,t)}{\partial y} = -\frac{\mathcal{H}}{\kappa} T(x,H,t)$$

where $\mathcal{H}$ is the convective heat transfer coefficient. These boundary conditions are illustrated in Figure 6.

Using the above mixed boundary conditions, the analytical solution to Eq. (3) for this problem can be shown to be [22]

$$T(x,y,t) = 4T_0 \sum_{k=1}^{\infty} \sum_{l=1}^{\infty} \frac{\overline{\mathcal{H}}^2 \exp\left[-\alpha_D\left(\beta_k^2 + \gamma_l^2\right)t\right] \cos(\beta_k x) \cos(\gamma_l y)}{\left[L(\beta_k^2 + \overline{\mathcal{H}}^2) + \overline{\mathcal{H}}\right]\left[H(\gamma_l^2 + \overline{\mathcal{H}}^2) + \overline{\mathcal{H}}\right] \cos(\beta_k L) \cos(\gamma_l H)} \tag{20}$$

where $\overline{\mathcal{H}} = \mathcal{H}/\kappa$, and β_k and γ_l are the positive roots to the transcendental equations

$$\beta_k \tan(\beta_k L) = \frac{\mathcal{H}}{\kappa} \quad \text{and} \quad \gamma_l \tan(\gamma_l H) = \frac{\mathcal{H}}{\kappa} \tag{21}$$

In the following simulation, we take $\alpha_D = 1\text{cm}^2/\text{s}$, $\kappa = 1$ W/cm K, and $\mathcal{H} = 0.1$ W/cm^2 K for the diffusivity, conductivity and convective heat transfer coefficient, respectively, as well as $T_0 = 100°\text{C}$.

The evolution of the temperature profile according to Eq. (20) is plotted in Figure 7 for times $t = 0.5$, $t = 1$, $t = 4$, and $t = 8$ s. As before, the SPH governing heat transfer equation is expressed implicitly by Eq. (18). The SPH boundary conditions were written using Eq. (9) for the boundary temperature gradients, where a factor of 2 was added to balance the one-sided nature of the gradient at the boundary. Written explicitly for each boundary surface in Cartesian coordinates, we obtain

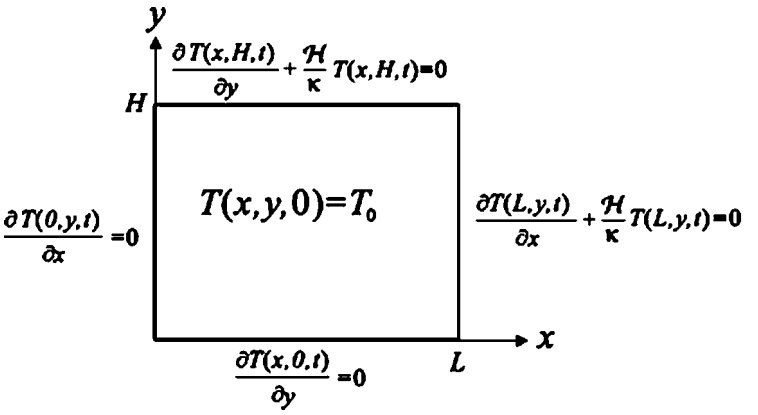

Figure 6. A 2-D (x, y) spatial domain with temperature boundary and initial conditions.

Downloaded By: [ANKOS Consortium] At: 10:15 18 January 2008

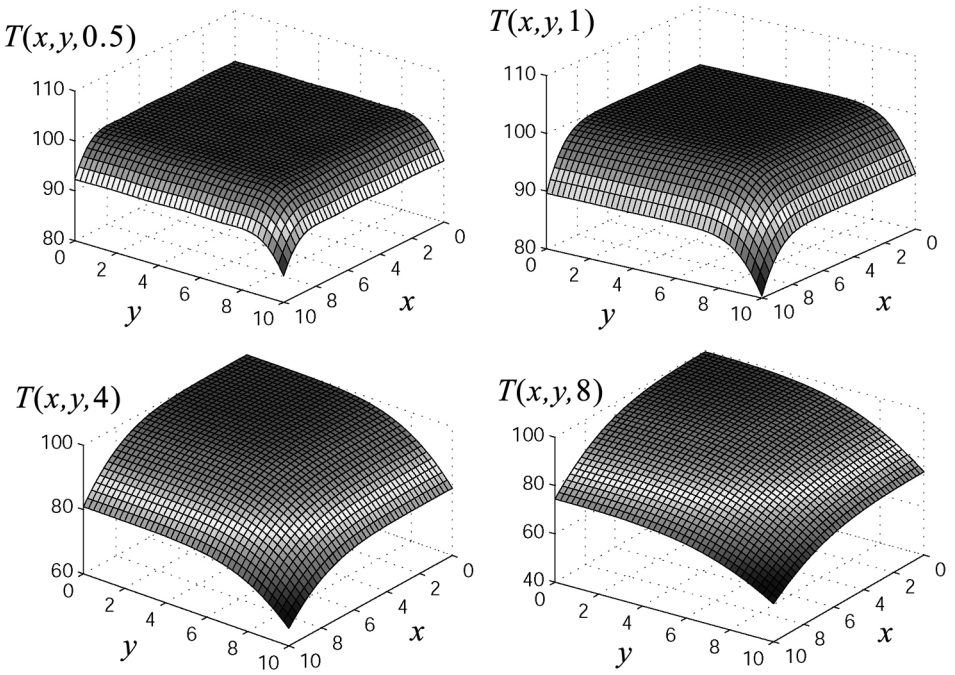

Figure 7. Analytical temperature profile at times $t = 0.5$, $t = 1$, $t = 4$, and $t = 8$ s found from Eq. (20).

the boundary conditions that must be satisfied for all time as

$$\left\langle \frac{\partial T_i(0,y,t)}{\partial x} \right\rangle = \sum_{j=1 j\neq i}^{N} 2\frac{m_j}{\rho_i}(T_j - T_i)\frac{\partial W(x_{ij},h_{ij})}{\partial x_i} = 0$$

$$\left\langle \frac{\partial T_i(x,0,t)}{\partial y} \right\rangle = \sum_{j=1 j\neq i}^{N} 2\frac{m_j}{\rho_i}(T_j - T_i)\frac{\partial W(x_{ij},h_{ij})}{\partial y_i} = 0$$

and

$$\left\langle \frac{\partial T_i(L,y,t)}{\partial x} \right\rangle = \sum_{j=1 j\neq i}^{N} 2\frac{m_j}{\rho_i}(T_j - T_i)\frac{\partial W(x_{ij},h_{ij})}{\partial x_i} = -\frac{\mathcal{H}}{\kappa}T_i(L,y,t)$$

$$\left\langle \frac{\partial T_i(x,H,t)}{\partial y} \right\rangle = \sum_{j=1 j\neq i}^{N} 2\frac{m_j}{\rho_i}(T_j - T_i)\frac{\partial W(x_{ij},h_{ij})}{\partial y_i} = -\frac{\mathcal{H}}{\kappa}T_i(x,H,t)$$

where in this case i is the boundary particle of interest.

Using the implicit Crank-Nicolson approach, the SPH temperature contours were found up to a time of $t = 8$ s, and are given along with the analytical solution

Downloaded By: [ANKOS Consortium] At: 10:15 18 January 2008

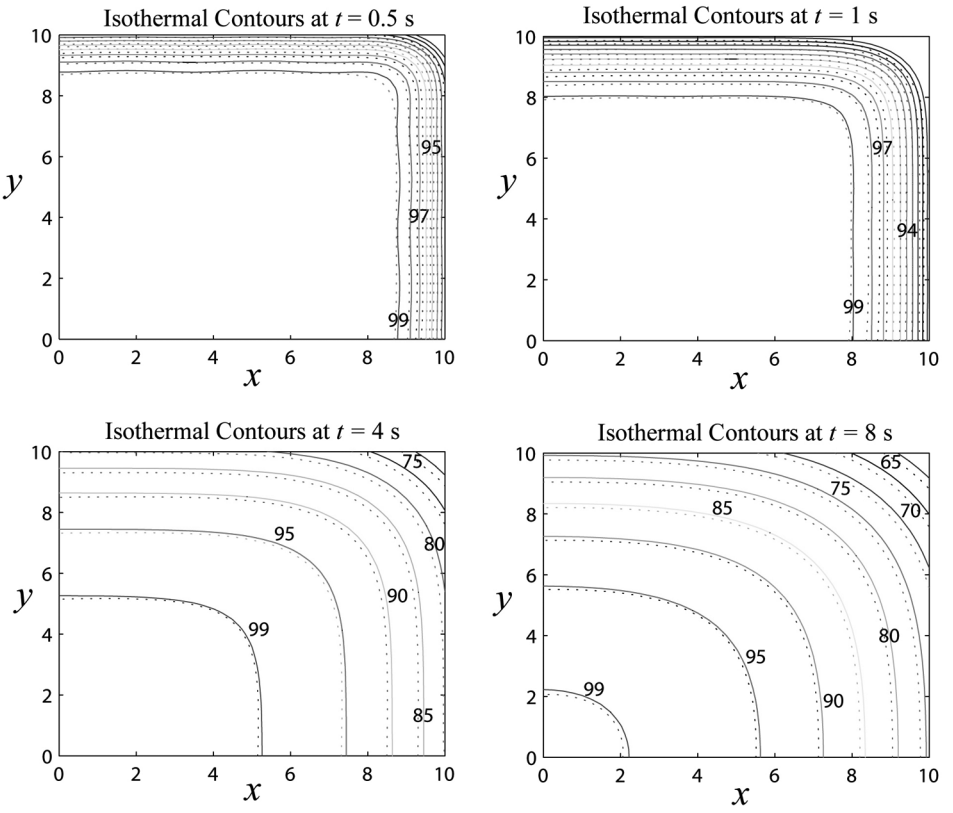

Figure 8. Isothermal contours at times $t = 0.5$, $t = 1$, $t = 4$, and $t = 8$ s using the Crank-Nicolson implicit time-stepping scheme.

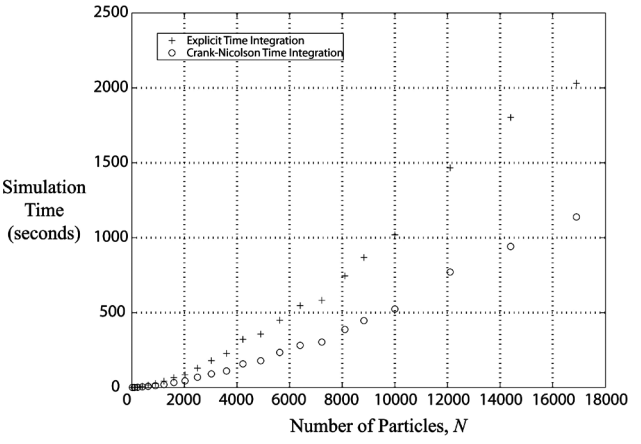

Figure 9. Simulation times versus number of SPH particles for explicit and Crank-Nicolson time integration schemes.

Downloaded By: [ANKOS Consortium] At: 10:15 18 January 2008

in Figure 8. In addition to the above simulations, testing was carried out in order to determine the computational time dependence on the number of SPH particles used. These tests incorporated simulations using both explicit and Crank-Nicolson time integration schemes for a simulation to $t = 0.5$ s. The result is given in Figure 9.

It was observed that the Crank-Nicolson implicit approach did not produce an obvious increase in solution accuracy compared with explicit time stepping. However, the Crank-Nicolson time step was half of that required by the explicit technique given by Eq. (12) to produce equivalent results. However, it was found that in the explicit approach, if the time step was greater than that permitted by Eq. (12), the solution broke down and did not converge. For these 2-D problems, the Crank-Nicolson solutions were unconditionally stable.

5. TRANSIENT CONDUCTION MODELING OF SEMICONDUCTOR CRYSTAL GROWTH

A liquid-phase diffusion (LPD) $Si_{0.05}Ge_{0.95}$ crystal growth simulation has been carried out, using a mesh-dependent finite-volume approach [23, 24]. However, in crystal growth simulations one must track the solid/liquid material interface as the growth progresses, which is very cumbersome due to the mesh adaptations required at each time step. Therefore, SPH is currently being investigated as an alternative simulation approach to crystal growth modeling, as no mesh is required in SPH.

LPD is a solution growth technique within the family of directional solidification. In this technique, the solvent material (Ge) is located between a single-crystal substrate (Ge) and polycrystalline source material (Si). The charge materials are contained in a quartz crucible and are exposed to an axial temperature gradient. Initially all charge materials are solid. As the system is heated to the growth temperature, the solvent Ge melts whereas the substrate melts partially and the silicon remains solid due its higher melting temperature. The solvent starts dissolving source material according to the binary SiGe phase diagram, hence producing the SiGe liquid phase. Silicon species are then transported toward the Ge substrate through diffusion and convection. When the liquid mixture in the vicinity of the growth interface becomes supersaturated, solidification takes place due to constitutional supercooling, thereby producing a single crystal. The silicon depletion in the solution is then replenished by the dissolution of source material. A more detailed description of the LPD system is available in the literature [23].

In Figure 10, the computational geometry is presented along with the representative thermal profile. A portion of the growth zone is covered by an annular insulator to allow a steep thermal profile in the vicinity of the growth interface. Here, the liquid phase represents a dilute binary mixture of silicon (solute) and germanium (solvent). The binary mixture is assumed to be a heat conducting incompressible Newtonian fluid. The solid phases, Ge single-crystal substrate, silicon source, and the quartz crucible, are considered to be heat-conducting rigid materials. The interface between the substrate and liquid is referred to as the growth interface, and the one between the liquid and source is the dissolution interface.

Figure 11 illustrates the two-dimensional SPH and finite-volume domains used to discretize the LPD crystal growth system. All dimensions are given in meters.

Downloaded By: [ANKOS Consortium] At: 10:15 18 January 2008

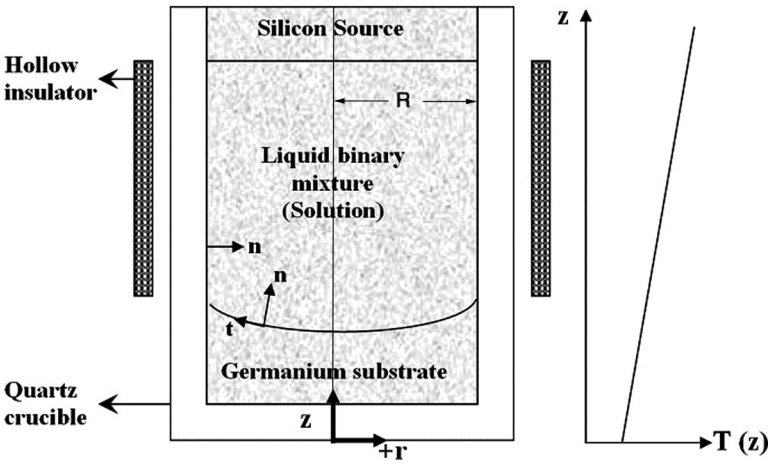

Figure 10. Computational domain of the LPD crystal growth system.

Here, the total number of particles used was $N = 2{,}754$, where the initial smoothing length was taken as $h = 0.5$ mm. The quartz crucible is represented by • particles, ○ particles represent the SiGe solution, and □ and ◇ particles represent the Ge substrate and Si source particles, respectively. As before, the ∗ symbol denotes particles that lie on the domain boundary.

For the finite-volume simulation, the respective mesh sizes for each material region are given in Table 1.

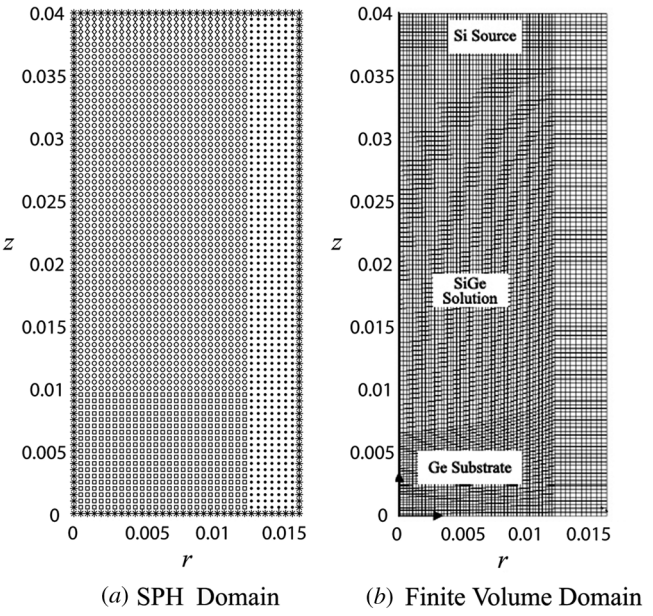

Figure 11. SPH and finite-volume domains for LPD simulation.

Downloaded By: [ANKOS Consortium] At: 10:15 18 January 2008

Table 1. LPD finite-volume simulation mesh sizes

Domain region	Mesh size
Si source	10×50
SiGe solution	80×50
Ge substrate	30×50
Quartz ampoule	$1{,}200 \times 10$

It has been shown [25] that the thermal profile may be computed independently of the flow field in liquid-phase diffusion crystal growth. That is, even though particles will move during the simulation according to the solution of the Navier–Stokes equations, this convective flow will not have a significant effect on the temperature field. This assumption was deduced from a dimensional analysis, where the computed Prandtl number, a ratio between convective and conductive effects, was found to be 0.0075 for the LPD system. As long as the Prandtl number is significantly less than one, the thermal transport across the solution is dominated by conduction, as opposed to the convective transport of fluid.

The thermal boundary conditions for the vertical wall, and the top and bottom surfaces of the quartz crucible, are modeled with the equation

$$-\kappa_S \frac{\partial T}{\partial n} = \mathcal{H}[T - T_f(z)] \tag{20}$$

where $T_f(z)$ is the experimentally obtained ambient temperature inside the furnace along the quartz ampoule wall or on the top and bottom surfaces, $\mathcal{H}$ is the modified heat transfer coefficient, including the contribution of convective and radiative effects on the heat transfer. The modified heat transfer coefficient was approximated using preliminary experimental results, such as the measured thermal profile, solute distribution in a grown crystal, and the position of the initial growth interface [24]. In addition, perfect thermal contact at the melt–ampoule, crystal–ampoule, and inner–outer crucible was assumed. At these boundaries, the heat flux was assumed to be continuous.

Table 2 lists the numerical values for the physical parameters used in the current model [25]. As well, since there are several materials present in the LPD system, the particle conductivity was modeled according to

$$\kappa_i \to \frac{2\kappa_i \kappa_j}{\kappa_i + \kappa_j} \tag{23}$$

derived by Monaghan and Cleary [19].

Table 2. Physical properties of the LPD system

Parameter	Si source at $T = 1,300$ K	Ge substrate at $T = 1,210$ K	SiGe liquid	Quartz
c_p (J/kg K)	967	396.1	380–406	1,200
κ (W/m K)	23.7	10.60	42.8	2.0
ρ (kg/m^3)	2,301.6	5,323	5,633	2,200

Downloaded By: [ANKOS Consortium] At: 10:15 18 January 2008

Use of the substitution equation (23) to model material regions having dissimilar thermal conductivities is a significant advantage of SPH over traditional finite-volume approaches. In the finite-volume simulations, the interface between two materials is required to have a boundary condition such that the heat flux is continuous. Computationally speaking, this approach is more expensive in terms of an additional boundary treatment within the computational domain. Alternatively, use of the SPH conductivity eliminates the need for special material treatment within the computational domain, as well as greatly simplifies the implementation.

Figure 12 illustrates the SPH and finite-volume [25] solutions to the thermal profile at $t = 0.5$ h, with all temperatures given in kelvin. As before, a Crank-Nicolson implicit time integration was used, allowing a time step of $\Delta t = 0.5$ s. The black lines represent material boundaries, with the concave lines indicating the computed growth interface.

Figure 12*a* shows the SPH computed temperature distributions in the substrate, solution, source, and quartz crucible for 0.5 h of growth time. As can be seen from Figure 12*a*, the initial growth interface deformed according to a reference isothermal line (the melting temperature of germanium, $T = 1211.45$ K) and is of a concave shape. The formation of a concave interface could be attributed to several reasons. The large mismatch in thermal conductivities of the substrate, solution, and surrounding quartz crucible bends isothermal lines in the vicinity of the interface. Recalling the experimental configuration in Figure 10, there is an annular insulator material located inside the furnace, which encompasses the quartz crucible with a 3–5-mm clearance. The insulator material spans from approximately 5 mm above the substrate to the bottom of the source material. The convective heat transfer in this semi-insulated region is handled by a proper estimate for the heat transfer coefficient, including both radiative and convective heat transfer. The presence of

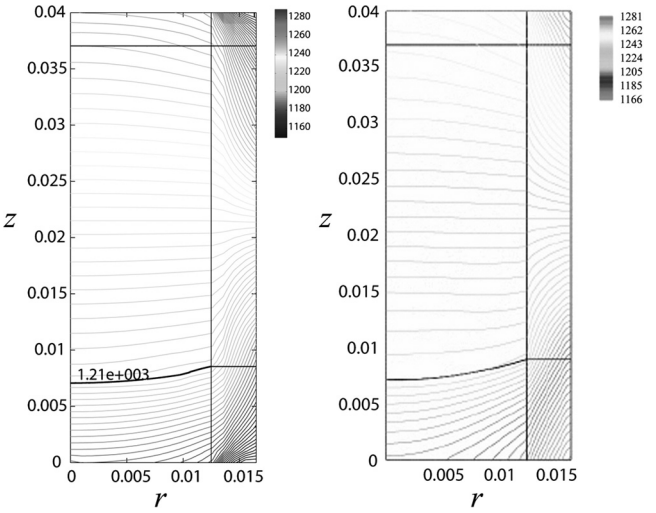

Figure 12. SPH and finite-volume temperature field at $t = 0.5$ h.

Downloaded By: [ANKOS Consortium] At: 10:15 18 January 2008

a ring-shaped insulator material distorts the isothermal lines around the boundary between the insulated and uninsulated regions. Furthermore, the convective heat transfer from the bottom of the crucible to the surrounding furnace atmosphere is smaller than that from the periphery of the ampoule due to the presence of a hollow quartz pedestal underneath the crucible. Away from the substrate and source material, thermal lines are almost flat due to being inside the insulated region. In the source material, thermal lines are convex since the top of the source material is in contact with the vacuum environment; therefore, heat transfer from the surroundings to the source material through its surface is less than that from its periphery through the quartz crucible. As for the thermal profile nearby the dissolution interface, it has a convex shape and large thermal gradients. A convex thermal profile can also be reasoned out by envisaging the difference in the thermal boundary conditions between the regions with and without insulation. In addition, there is a large mismatch in thermal conductivities of the solution, source, and crucible as well. Upon comparing the simulation results obtained by SPH and finite-volume approaches, it can easily be concluded that there is very good agreement between these techniques. This finding confirms that the use of Eq. (23) to model thermal conductivities is indeed acceptable for crystal growth simulations, and did not have a negative effect on solution accuracy.

6. CONCLUDING REMARKS

The motivation behind this work is to develop a mathematical model to solve transport equations for the simulation of the LPD growth process by using the SPH approach. The mathematical simulation of the crystal growth process necessitates long computation times (hours), due to the slow nature of the crystal growth process. SPH has been successfully used to model many engineering problems which can be resolved in short time spans. Therefore, explicit time stepping was sufficient for these applications. In order to put SPH into the category of other computational techniques, larger time steps are required, which can be achieved by employing an implicit time-stepping approach. In this article, we have presented two different heat transfer problems with simple and complex boundary conditions to validate that the developed code produces results which agree with the analytical solutions. The temperature distribution in the LPD growth system was then computed using SPH. It was found that the SPH and finite-volume results were in good agreement.

REFERENCES

1. G. R. Liu and M. B. Liu, *Smoothed Particle Hydrodynamics: A Meshfree Particle Method*, p. 18, World Scientific Publishing Co., Singapore, 2003.
2. Y. L. Wu, G. R. Liu, and Y. T. Gu, Application of Meshless Local Petrov-Galerkin (MLPG) Approach to Simulation of Incompressible Flow, *Numer. Heat Transfer B*, vol. 48, pp. 459–475, 2005.
3. I. V. Singh, K. Sandeep, and R. Prakash, Heat Transfer Analysis of Two-Dimensional Fins Using a Meshless Element Free Galerkin Method, *Numer. Heat Transfer A*, vol. 44, pp. 73–84, 2003.

Downloaded By: [ANKOS Consortium] At: 10:15 18 January 2008

4. I. V. Singh, Meshless EFG Method in Three-Dimensional Heat Transfer Problems: A Numerical Comparison, Cost and Error Analysis, *Numer. Heat Transfer A*, vol. 46, pp. 199–220, 2004.
5. I. V. Singh and P. K. Jain, Parallel Meshless EFG Solution for Fluid Flow Problems, *Numer. Heat Transfer B*, vol. 48, pp. 45–66, 2005.
6. J. Y. Tan, L. H. Liu, and B. X. Li, Least-Squares Collocation Meshless Approach for Coupled Radiative and Conductive Heat Transfer, *Numer. Heat Transfer B*, vol. 49, pp. 179–195, 2006.
7. T. Sophy, H. Sadat, and C. Prax, A Meshless Formulation for Three-Dimensional Laminar Natural Convection, *Numer. Heat Transfer B*, vol. 41, pp. 433–445, 2002.
8. L. B. Lucy, A Numerical Approach to the Testing of the Fission Hypothesis, *Astro. J.*, vol. 82, pp. 1013–1024, 1977.
9. R. A. Gingold and J. J. Monaghan, Smooth Particle Hydrodynamics: Theory and Application to Non-Spherical Stars, *Mon. Not. R. Astron. Soc.*, vol. 181, p. 375, 1977.
10. L. D. G. Sigalotti, J. Klapp, E. Sira, Y. Meleán, and A. Hasmy, SPH Simulations of Time-Dependent Poiseuille Flow at Low Reynolds Numbers, *J. Comput. Phys.*, vol. 191, pp. 622–638, 2003.
11. Y. Zhu and P. J. Fox, Smoothed Particle Hydrodynamics Model for Diffusion through Porous Media, *Transport Porous Media*, vol. 43, pp. 441–471, 2001.
12. M. B. Liu, G. R. Liu, and K. Y. Lam, A One-Dimensional Meshfree Particle Formulation for Simulating Shock Waves, *Shock Waves*, vol. 13, pp. 201–211, 2003.
13. A. Colagrossi and M. Landrini, Numerical Simulation of Interfacial Flows by Smoothed Particle Hydrodynamics, *J. Comput. Phys.*, vol. 191, pp. 448–475, 2003.
14. P. Cleary, J. Ha, V. Alguine, and T. Nguyen, Flow Modelling in Casting Processes, *Applied Mathematical Modelling*, vol. 26, pp. 171–190, 2002.
15. S. Dost and Z. Qin, A Numerical Simulation Model for Liquid Phase Electroepitaxial Growth of GaInAs, *J. Crystal Growth*, vol. 187, pp. 51–64, 1998.
16. Y. C. Liu, Y. Okano, and S. Dost, The Effect of Applied Magnetic Field on Flow Structures in Liquid Phase Electroepitaxy—A Three-Dimensional Simulation Model, *J. Crystal Growth*, vol. 244, pp. 12–26, 2002.
17. S. Dost, Y. Liu, and B. Lent, A Numerical Simulation Study for the Effect of Applied Magnetic Field in Liquid Phase Electroepitaxy, *J. Crystal Growth*, vol. 240, pp. 39–51, 2002.
18. J. J. Monaghan, Implicit SPH Drag and Dusty Gas Dynamics, *J. Comput. Phys.*, vol. 138, pp. 801–820, 1997.
19. P. W. Cleary and J. J. Monaghan, Conduction Modelling Using Smoothed Particle Hydrodynamics, *J. Comput. Phys.*, vol. 148, pp. 235–236, 1999.
20. J. Bonet and M. X. Rodriguez-Paz, Hamiltonian Formulation of the Variable-*h* SPH Equations, *J. Comput. Phys.*, vol. 209, pp. 541–558, 2005.
21. S. J. Cummins and M. Rudman, An SPH Projection Method, *J. Comput. Phys.*, vol. 152, pp. 584–607, 1999.
22. M. N. Özişik, *Heat Conduction*, 2nd ed., p. 75, Wiley, New York, 1993.
23. M. Yildiz, S. Dost, and B. Lent, Growth of Bulk SiGe Single Crystals by Liquid Phase Diffusion, *J. Crystal Growth*, vol. 280, pp. 151–160, 2005.
24. M. Yildiz and S. Dost, A Continuum Model for the Liquid Phase Diffusion Growth of Bulk SiGe Single Crystals, *Int. J. Eng. Sci.*, vol. 43, pp. 1059–1080, 2005.
25. M. Yildiz, A Combined Experimental and Modelling Study for the Growth of Si_xGe_{1-x} Single Crystals by Liquid Phase Diffusion (LPD), Ph.D. thesis, The University of Victoria, Victoria, BC, Canada, 2005.

Downloaded By: [ANKOS Consortium] At: 10:15 18 January 2008

APPENDIX

In general, a scalar function $f(x_i^1, x_i^2, , x_i^n) = f(x_i^\beta)$ of the position vector x_i^β can be represented by a Taylor series, expanded around the vector location x_j^β as

$$f(x_i^\beta) = \sum_{k=0}^{\infty} \left[\frac{1}{k!} \left[x_{ij}^\gamma ()_{;\gamma} \right]^k f(x_i^\beta) \Big|_{x_i^\beta = x_j^\beta} \right] \tag{A.1}$$

where the $()_{;\gamma}$ operator denotes *covariant differentiation* with respect to coordinate x_i^γ. If we expand Eq. (A.1), we obtain, explicitly,

$$f(x_i^\beta) = f(x_j^\beta) + x_{ij}^\gamma f_{;\gamma}(x_j^\beta) + \frac{x_{ij}^\gamma x_{ij}^\lambda}{2} f_{;\gamma\lambda}(x_i^\beta) \Big|_{x_i^\beta = x_j^\beta} + \cdots \tag{A.2}$$

since the difference vector x_{ij}^γ is a constant and can be pulled out of the covariant derivative expression.

To find the SPH approximation for the Laplacian operator, we begin by multiplying the Taylor series expansion of Eq. (A.2) with the term $x_{ij}^\alpha W_{;\alpha}(x_{ij}, h)/g_{\mu\nu} x_{ij}^\mu x_{ij}^\nu$ producing

$$\begin{aligned} \frac{\left[f(x_i^\beta) - f(x_j^\beta) \right] x_{ij}^\alpha}{g_{\mu\nu} x_{ij}^\mu x_{ij}^\nu} W_{;\alpha}(x_{ij}, h) = {} & \frac{x_{ij}^\gamma x_{ij}^\alpha}{g_{\mu\nu} x_{ij}^\mu x_{ij}^\nu} W_{;\alpha}(x_{ij}, h) f_{;\gamma}(x_j^\beta) \\ & + \frac{x_{ij}^\gamma x_{ij}^\lambda x_{ij}^\alpha}{2 g_{\mu\nu} x_{ij}^\mu x_{ij}^\nu} W_{;\alpha}(x_{ij}, h) f_{;\gamma\lambda}(x_i^\beta) \Big|_{x_i^\beta = x_j^\beta} + \cdots \end{aligned}$$

We then integrate over all three-dimensional space in $d\Omega = dx_i^\beta$ coordinates, which yields (after noting that the first integral term has an integrand with an odd function, and therefore goes to zero when integrated over all space)

$$\iiint_\Omega \frac{\left[f(x_i^\beta) - f(x_j^\beta) \right] x_{ij}^\alpha}{g_{\mu\nu} x_{ij}^\mu x_{ij}^\nu} W_{;\alpha}(x_{ij}, h) d\Omega = \frac{f_{;\gamma\lambda}(x_j^\beta)}{2} \iiint_\Omega \frac{x_{ij}^\gamma x_{ij}^\lambda x_{ij}^\alpha}{g_{\mu\nu} x_{ij}^\mu x_{ij}^\nu} W_{;\alpha}(x_{ij}, h) d\Omega \tag{A.3}$$

up to second order. Expanding the integrand on the right-hand side using the product rule gives

$$\frac{x_{ij}^\gamma x_{ij}^\lambda x_{ij}^\alpha}{g_{\mu\nu} x_{ij}^\mu x_{ij}^\nu} W_{;\alpha}(x_{ij}, h) = \left(\frac{x_{ij}^\gamma x_{ij}^\lambda x_{ij}^\alpha}{g_{\mu\nu} x_{ij}^\mu x_{ij}^\nu} W(x_{ij}, h) \right)_{;\alpha} - W(x_{ij}, h) \left(\frac{x_{ij}^\gamma x_{ij}^\lambda x_{ij}^\alpha}{g_{\mu\nu} x_{ij}^\mu x_{ij}^\nu} \right)_{;\alpha}$$

which produces

$$\begin{aligned} \iiint_\Omega \frac{x_{ij}^\gamma x_{ij}^\lambda x_{ij}^\alpha}{g_{\mu\nu} x_{ij}^\mu x_{ij}^\nu} W_{;\alpha}(x_{ij}, h) d\Omega = {} & \iiint_\Omega \left(\frac{x_{ij}^\gamma x_{ij}^\lambda x_{ij}^\alpha}{g_{\mu\nu} x_{ij}^\mu x_{ij}^\nu} W(x_{ij}, h) \right)_{;\alpha} d\Omega \\ & - \iiint_\Omega W(x_{ij}, h) \left(\frac{x_{ij}^\gamma x_{ij}^\lambda x_{ij}^\alpha}{g_{\mu\nu} x_{ij}^\mu x_{ij}^\nu} \right)_{;\alpha} d\Omega \end{aligned}$$

Downloaded By: [ANKOS Consortium] At: 10:15 18 January 2008

for the integral on the right-hand side of Eq. (A.3). Using the divergence theorem for the first integral on the right-hand side of the above equation gives

$$\iiint_{\Omega} \frac{x_{ij}^{\gamma} x_{ij}^{\lambda} x_{ij}^{\alpha}}{g_{\mu\nu} x_{ij}^{\mu} x_{ij}^{\nu}} W_{;\alpha}(x_{ij}, h) d\Omega = \iint_{S} \left(\frac{x_{ij}^{\gamma} x_{ij}^{\lambda} x_{ij}^{\alpha}}{g_{\mu\nu} x_{ij}^{\mu} x_{ij}^{\nu}} W(x_{ij}, h) \right) n_{\alpha} dS - \iiint_{\Omega} W(x_{ij}, h) \left(\frac{x_{ij}^{\gamma} x_{ij}^{\lambda} x_{ij}^{\alpha}}{g_{\mu\nu} x_{ij}^{\mu} x_{ij}^{\nu}} \right)_{;\alpha} d\Omega$$

Once again, we have the surface integral vanishing for all interior particles since the kernel goes to zero, leaving

$$\iiint_{\Omega} \frac{x_{ij}^{\gamma} x_{ij}^{\lambda} x_{ij}^{\alpha}}{g_{\mu\nu} x_{ij}^{\mu} x_{ij}^{\nu}} W_{;\alpha}(x_{ij}, h) d\Omega = - \iiint_{\Omega} W(x_{ij}, h) \left(\frac{x_{ij}^{\gamma} x_{ij}^{\lambda} x_{ij}^{\alpha}}{g_{\mu\nu} x_{ij}^{\mu} x_{ij}^{\nu}} \right)_{;\alpha} d\Omega \tag{A.4}$$

Expansion of the derivative in the integrand of Eq. (A.4) yields

$$\begin{aligned} \left(\frac{x_{ij}^{\gamma} x_{ij}^{\lambda} x_{ij}^{\alpha}}{g_{\mu\nu} x_{ij}^{\mu} x_{ij}^{\nu}} \right)_{;\alpha} &= \frac{1}{g_{\mu\nu} x_{ij}^{\mu} x_{ij}^{\nu}} \left(x_{ij}^{\gamma} x_{ij}^{\lambda} x_{ij}^{\alpha} \right)_{;\alpha} + x_{ij}^{\gamma} x_{ij}^{\lambda} x_{ij}^{\alpha} \left(\frac{1}{g_{\mu\nu} x_{ij}^{\mu} x_{ij}^{\nu}} \right)_{;\alpha} \\ &= \frac{\delta_{\alpha}^{\gamma} x_{ij}^{\lambda} x_{ij}^{\alpha} + x_{ij}^{\gamma} \delta_{\alpha}^{\lambda} x_{ij}^{\alpha} + x_{ij}^{\gamma} x_{ij}^{\lambda} \delta_{\alpha}^{\alpha}}{g_{\mu\nu} x_{ij}^{\mu} x_{ij}^{\nu}} - \frac{x_{ij}^{\gamma} x_{ij}^{\lambda} x_{ij}^{\alpha} g_{\sigma\psi} \left(x_{ij;\alpha}^{\sigma} x_{ij}^{\psi} + x_{ij}^{\sigma} x_{ij;\alpha}^{\psi} \right)}{g_{\mu\nu} x_{ij}^{\mu} x_{ij}^{\nu} g_{\eta\zeta} x_{ij}^{\eta} x_{ij}^{\zeta}} \\ &= \frac{5 x_{ij}^{\gamma} x_{ij}^{\lambda}}{g_{\mu\nu} x_{ij}^{\mu} x_{ij}^{\nu}} - \frac{x_{ij}^{\gamma} x_{ij}^{\lambda} x_{ij}^{\alpha} g_{\alpha\psi} x_{ij}^{\psi} + x_{ij}^{\gamma} x_{ij}^{\lambda} x_{ij}^{\alpha} g_{\sigma\alpha} x_{ij}^{\sigma}}{g_{\mu\nu} x_{ij}^{\mu} x_{ij}^{\nu} g_{\eta\zeta} x_{ij}^{\eta} x_{ij}^{\zeta}} \\ &= \frac{3 x_{ij}^{\gamma} x_{ij}^{\lambda}}{g_{\mu\nu} x_{ij}^{\mu} x_{ij}^{\nu}} \end{aligned} \tag{A.5}$$

Now, using Eq. (A.5) in Eq. (A.4) gives the result

$$\iiint_{\Omega} \frac{x_{ij}^{\gamma} x_{ij}^{\lambda} x_{ij}^{\alpha}}{g_{\mu\nu} x_{ij}^{\mu} x_{ij}^{\nu}} W_{;\alpha}(x_{ij}, h) d\Omega = - \iiint_{\Omega} \frac{3 x_{ij}^{\gamma} x_{ij}^{\lambda}}{g_{\mu\nu} x_{ij}^{\mu} x_{ij}^{\nu}} W(x_{ij}, h) d\Omega \tag{A.6}$$

The second-order tensor in the above equation must be an isotropic tensor, since the kernel is a symmetric function multiplied by an even function. An isotropic tensor is one that can be written in terms of a constant c and the Kronecker delta as $c\delta_{\sigma}^{\gamma}$. However, since the integral on the right-hand side of Eq. (A.6) has two contravariant free indices γ and λ, we raise an index of our isotropic tensor with multiplication of the metric, so that

$$- \iiint_{\Omega} \frac{3 x_{ij}^{\gamma} x_{ij}^{\lambda}}{g_{\mu\nu} x_{ij}^{\mu} x_{ij}^{\nu}} W(x_{ij}, h) d\Omega = c g^{\lambda\sigma} \delta_{\sigma}^{\gamma} \tag{A.7}$$

Downloaded By: [ANKOS Consortium] At: 10:15 18 January 2008

is the appropriate representation of the isotropic tensor. The constant c can be found from inner multiplication of the above equation with the metric $g_{\gamma\lambda}$, producing

$$-g_{\gamma\lambda}\iiint_{\Omega}\frac{3x_{ij}^{\gamma}x_{ij}^{\lambda}}{g_{\mu\nu}x_{ij}^{\mu}x_{ij}^{\nu}}W(x_{ij},h)d\Omega = cg_{\gamma\lambda}g^{\lambda\sigma}\delta_{\sigma}^{\gamma} = c\delta_{\gamma}^{\gamma} \tag{A.8}$$

which, since the kernel is normalized, yields $c = -1$. Substituting this value of c into Eq. (A.7), and using the results of Eqs. (A.6), and (A.3), we obtain, up to second order,

$$\iiint_{\Omega}\frac{\left[f(x_i^{\beta}) - f(x_j^{\beta})\right]x_{ij}^{\alpha}}{g_{\mu\nu}x_{ij}^{\mu}x_{ij}^{\nu}}W_{;\alpha}(x_{ij},h)d\Omega = -\left.\frac{g^{\gamma\lambda}f_{;\gamma\lambda}(x_i^{\beta})}{2}\right|_{x_i^{\beta}=x_j^{\beta}}$$

which can be rewritten as

$$\left\langle g^{\gamma\lambda}f_{;\gamma\lambda}(x_j^{\beta})\right\rangle = 2\iiint_{\Omega}\frac{\left[f(x_j^{\beta}) - f(x_i^{\beta})\right]x_{ij}^{\alpha}}{g_{\mu\nu}x_{ij}^{\mu}x_{ij}^{\nu}}W_{;\alpha}(x_{ij},h)d\Omega$$

Our final result for the SPH Laplacian of a scalar field is written in terms of particle i by letting $i \to j$ and $j \to i$, noting that $x_{ij}^{\beta} = -x_{ji}^{\beta}$ and $W_{;\alpha} = -W_{;\alpha_j}$, to yield

$$\left\langle g^{\gamma\lambda}f_{;\gamma\lambda}(x_i^{\beta})\right\rangle = 2\iiint_{\Omega}\frac{\left[f(x_i^{\beta}) - f(x_j^{\beta})\right]x_{ij}^{\alpha}}{g_{\mu\nu}x_{ij}^{\mu}x_{ij}^{\nu}}W_{;\alpha}(x_{ij},h)d\Omega \tag{A.9}$$

where all covariant derivatives in the above equation are with respect to x_i^{β} coordinates.

View publication stats